



Observed source parameters for dynamic rupture with non-uniform initial stress and relatively high fracture energy

Nick Beeler^{a,*}, Brian Kilgore^a, Art McGarr^a, Joe Fletcher^a, John Evans^a, Steven R. Baker^b

^a US Geological Survey, Menlo Park, CA, USA

^b Naval Postgraduate School, Monterey, CA, USA

ARTICLE INFO

Article history:

Received 22 March 2011

Received in revised form

26 October 2011

Accepted 10 November 2011

Available online 16 December 2011

Keywords:

Dynamic rupture

Friction

Stress drop

Efficiency

Fracture energy

ABSTRACT

We have conducted dynamic rupture propagation experiments to establish the relations between in-source stress drop, fracture energy and the resulting particle velocity during slip of an unconfined 2 m long laboratory fault at normal stresses between 4 and 8 MPa. To produce high fracture energy in the source we use a rough fault that has a large slip weakening distance. An artifact of the high fracture energy is that the nucleation zone is large such that precursory slip reduces fault strength over a large fraction of the total fault length prior to dynamic rupture, making the initial stress non-uniform. Shear stress, particle velocity, fault slip and acceleration were recorded coseismically at multiple locations along strike and at small fault-normal distances. Stress drop increases weakly with normal stress. Average slip rate depends linearly on the fault strength loss and on static stress drop, both with a nonzero intercept. A minimum fracture energy of 1.8 J/m² and a linear slip weakening distance of 33 μm are inferred from the intercept. The large slip weakening distance also affects the average slip rate which is reduced by in-source energy dissipation from on-fault fracture energy.

Because of the low normal stress and small per event slip (~86 μm), no thermal weakening such as melting or pore fluid pressurization occurs in these experiments. Despite the relatively high fracture energy, and the very low heat production, energy partitioning during these laboratory earthquakes is very similar to typical earthquake source properties. The product of fracture energy and fault area is larger than the radiated energy. Seismic efficiency is low at ~2%. The ratio of apparent stress to static stress drop is ~27%, consistent with measured overshoot. The fracture efficiency is ~33%. The static and dynamic stress drops when extrapolated to crustal stresses are 2–7.3 MPa and in the range of typical earthquake stress drops. As the relatively high fracture energy reduces the slip velocities in these experiments, the extrapolated average particle velocities for crustal stresses are 0.18–0.6 m/s. That these experiments are consistent with typical earthquake source properties suggests, albeit indirectly, that thermal weakening mechanisms such as thermal pressurization and melting which lead to near complete stress drops, dominate earthquake source properties only for exceptional events unless crustal stresses are low.

Published by Elsevier Ltd.

1. Introduction

The earthquake source is a three dimensional volume in which many inelastic processes may operate (e.g. frictional sliding, brittle rock fracture, dilatancy, melting, other phase changes, thermal expansion of pore fluid, hydrofracture, creation of new fracture surface energy, etc); only outside the source is rock predominantly elastic and able to transmit information unambiguously. Since earthquake seismology involves interpretation of elastodynamic

waves, the wavefield contains only indirect information about the details of processes operating within the source. It is the physical processes that operate in the source region to dissipate and store energy that limit the amount of energy that is available to be radiated and which ultimately cause damaging ground motions at the earth's surface.

To examine causal relationships in the source region among on-fault strength, stress drop and the resulting near-fault particle velocity during coseismic slip, in this report we describe rupture propagation experiments where stress drop, energy dissipation and across fault motions are measured coseismically. Using some guidance from seismology, our observations allow us to relate source properties to the resultant propagating displacements that

* Corresponding author.

E-mail address: nbeeler@usgs.gov (N. Beeler).

would lead to ground motion in a natural setting. Specifically, we find that particle velocities increase systematically with in-source strength loss or stress drop and that particle velocity decreases with increasing in-source fracture energy. To determine the implications of our experimental results for natural earthquake requires an extrapolation in normal stress from the few MPa stresses of the experiments to crustal stress, and an extrapolation in scale from the meter fault length of the experiments to the large earthquake ruptures relevant to seismic hazard. The stress extrapolation is straightforward but the scale extrapolation is not. Rather than undertake a literal rescaling of the results, instead we examine energy partitioning, particularly the relative amounts of energy that are radiated and that are dissipated as fracture energy in the source. These efficiencies allow us to compare our experimental observations with earthquakes of any scale and we find that our experiments are entirely consistent with typical earthquakes of all sizes.

Before describing the experimental procedures, the results and interpretations in detail, the remainder of this introduction contains two sections of background material from seismology for our experiments. The first introduces the expected relations among in-source fault strength, dissipation and the resulting particle velocity, drawn from the published literature. The second section covers energy partitioning during earthquakes and develops the particular efficiencies of radiated and fracture energy that are needed to compare our experiments to natural earthquakes. This latter introductory section draws both on well-known published work and some novel ideas unique to laboratory studies of dynamic rupture.

1.1. Expected relations between fault stress drop and near-fault particle velocity

Some expectations for particle velocity in our experiments are illustrated by simple theories of the earthquake source. For example, assuming that earthquake faulting can be represented by a discontinuity or narrow shear zone embedded in perfectly elastic surroundings (Fig. 1) the particle velocity measured just outside the source resulting from fault slip is related to the source stress change through Hooke's Law. The stress change $\Delta\sigma$ is proportional to the elastic strain, $\Delta\sigma = E\partial u/\partial x$ where u is shear displacement, u is one half the fault slip, E and x are the appropriate elastic constant and spatial coordinate respectively. Dimensionally, to consider relations between stress change and particle velocity the spatial coordinate can be replaced using the relation $dx = V_c dt$, where V_c is a characteristic velocity, leading to the general relationship

$$\dot{u} = \frac{\partial u}{\partial t} = \Delta\sigma \frac{V_c}{E}. \quad (0)$$

Among the specific theories that relate source stress change to the particle velocity, consider (0) in the context of Brune (1970) and

Ida (1973). If propagation effects are ignored such that the source slip produces a planar shear wave (Brune, 1970), then $dx = \beta dt$ where β is the shear wave speed. The appropriate elastic constant is the shear modulus μ . Thus, the near-field particle velocity associated with a stress change in the source is

$$\dot{u} \approx \Delta\sigma \frac{\beta}{\mu} \quad (1)$$

(Brune, 1970). If instead propagation effects are considered, at the tip of a propagating rupture $dx = V_r dt$ where V_r is the rupture velocity. For a simple consideration of in-plane shear the appropriate elastic constant is of the order of the shear modulus μ and

$$\dot{u} \approx \Delta\sigma \frac{V_r}{\mu} \quad (2)$$

(Ida, 1973).

Both (1) and (2) require a proportionality between source strength loss and the particle velocity indicating that the velocity is ultimately limited by the total amount of stored elastic energy available to be released. In these models (1) and (2), the available energy is that associated with the strength loss, $\Delta\sigma DA$, and all of it is radiated. Here D is total fault slip, A is fault area. Thus, knowing the limit to strength loss is sufficient for estimating the limit on near-fault particle velocity.

However, for natural earthquakes it is likely that only a fraction of energy associated with the strength loss is radiated. There is in-source dissipation if the fault strength drops gradually rather than abruptly, defining an on-fault 'fracture energy' (Ida, 1972; Andrews, 1976). If the surroundings aren't perfectly elastic, then there can be significant off fault yielding that dissipates energy as radiation propagates away from the fault (e.g., Andrews, 2005). In these cases these non-radiated energies are dissipated as heat or stored as latent heat within the source region, in which case reasonably we expect

$$\dot{u} = \frac{\partial u}{\partial t} < \Delta\sigma \frac{V_c}{E}. \quad (3)$$

Essentially, the purpose of the present study is to demonstrate and quantify the expectation equation (3) in a laboratory setting where source strength loss and particle velocity are measured directly.

1.2. Energy partitioning and efficiency

Explicit in the discussion preceding equation (3) is that near-source particle velocities depend on how much stored elastic energy is available to be released and how much of that available energy is actually partitioned into the radiated field. Because seismic measures of energy such as seismic moment increase with fault dimension squared, any laboratory scale experiment to test such seismologic concepts has to be extrapolated over many orders of magnitude following a non-linear scale to be comparable to real earthquakes. Instead of extrapolating in scale, an alternative is to compare energy in laboratory events to earthquakes by calculating efficiencies that define the relative amounts of radiated and source-dissipated energy. The necessary efficiencies for radiated energy, the Savage-Wood efficiency, and for fracture energy, the fracture efficiency are derived from a standard earthquake energy balance, as follows.

The total energy released during an earthquake is $E_T = \bar{\tau}M_o/\mu$ where $\bar{\tau}$ is the slip-averaged and spatially-averaged shear stress in the direction of shear offset, μ is the shear modulus and M_o is the seismic moment. Ignoring rotational and gravitational terms, the total energy E_T is partitioned between radiated energy E_R , and the sum of energy that is dissipated or stored within the source by

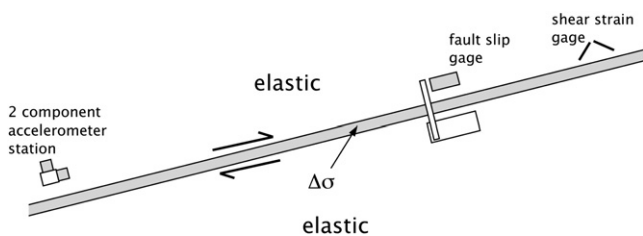


Fig. 1. A simple fault model consisting of a thin shear zone embedded in elastic surroundings. Shown also are near-fault and across-fault instrumentation as used in this study.

frictional heating, fracture, latent heats associated with phase transformations and other processes. An often used source representation is

$$E_T = E_R + E_k. \quad (4a)$$

For the case where all the dissipation occurs on the fault the dissipated energy is $E_k = \bar{\tau}_{sliding} M_0 / \mu$ where $\bar{\tau}_{sliding}$ is the displacement averaged fault strength. Expressing (4a) in terms of stress we have

$$\bar{\tau} = \bar{\tau}_{sliding} + \tau_a. \quad (4b)$$

where τ_a is the apparent stress, the stress measure of radiated energy $\tau_a = \mu E_R / M_0$. Rearranging (4b), the apparent stress can be written in terms of static stress drop and stress overshoot $\xi = (\bar{\tau}_{sliding} - \tau_1) / \Delta\tau_s$ (Savage and Wood, 1971; McGarr, 1999) as

$$\tau_a = \Delta\tau_s (0.5 - \xi). \quad (5)$$

The efficiency measure of radiated energy we will use to compare our laboratory observations to earthquakes, the Savage-Wood efficiency $\eta_{sw} = \tau_a / \Delta\tau_s$ follows, from equation (5). Since this efficiency is the ratio of two common seismologically measured source parameters, it is in principle easily estimated for large earthquakes. Low efficiency may be associated with earthquakes in which the slip speeds are low, such as for tsunamigenic events (e.g., Venkataraman and Kanamori, 2004). High efficiency earthquakes may be associated, for example, with self-healing pulses where apparent stress and the dynamic stress drop can exceed the static stress drop (Heaton, 1990).

A similar approach can be applied to estimate energy dissipation in the source that reduces the radiated energy. If for example fault strength drops linearly over some slip distance d^* and then subsequently remains constant with slip (linear slip weakening: Ida, 1972; Andrews, 1976), the associated energy per unit area (the fracture energy), $G_e = \Delta\tau d^* / 2$, is dissipated as heat or latent heat and is not available to be radiated. For linear slip weakening we can define a fracture stress τ_c as the difference between the average sliding resistance and the final sliding resistance, equivalently $\tau_c = G_e / D$ where D is total slip. The associated efficiency is the ratio of fracture energy times the fault area to the energy associated with the static stress drop $\eta_c = G_e / \Delta\tau_s D$, equivalently the ratio of the fracture stress to the static stress drop $\eta_c = \tau_c / \Delta\tau_s$.

We have conducted rupture propagation experiments on a large laboratory-scale fault in Sierra granite that has relatively high fracture energy to examine the relationships among strength loss, on-fault slip speed, near-fault particle velocity, and measures of coseismic energy partitioning. Ours is an extension of studies conducted by Okubo and Dieterich (1981, 1984) Lockner et al. (1982) and Lockner and Okubo (1983). Shear stress, particle velocity, fault slip and acceleration were recorded during dynamic rupture propagation at multiple locations along strike and at small fault-normal distances. Resulting empirical relations among source parameters are discussed and explained with reference to the predictions of simple theoretical models and qualitative seismological theory. Observed stress drops, peak and average slip speed, near-fault peak particle velocity, and fracture efficiency are compared with previous laboratory experiments and natural earthquakes. In particular, because we are able to measure directly both the causative fault strength losses and the resulting motions we are able to consider the implications of these experiments for near fault particle velocities of large hazardous earthquakes. We find generally that energy partitioning for these lab-scale earthquakes is consistent with typical earthquakes despite the high fracture energy: seismic efficiency is $\sim 2\%$, the ratio of apparent

stress to static stress drop is $\sim 27\%$, consistent with measured overshoot and with typical seismic observations, and the fracture efficiency is $\sim 33\%$, perhaps slightly higher but comparable with the limited seismic observations. When extrapolated to crustal stresses, predicted stress drops are a few MPa and average particle velocities are a few tenths of a meter per second.

2. Experiments

The experiments were conducted on a large biaxial press (Dieterich, 1981) (Fig. 2). The press accommodates samples $1.5 \times 1.5 \times 0.4$ m with a pre-cut fault surface along the diagonal, 45° to the long dimensions, with length and depth of 2×0.4 m, respectively. The load bearing elements are seven steel plates stacked and bolted together. The fault is loaded along the outward faces of the 1.5 m long sides of the fault blocks using four flat jacks filled with hydraulic oil and pressurized by servo control. Flat jacks on opposite sides see the same pressure; thus there are two orthogonal controlled forces applied to the blocks. There are Teflon plates between the frame and the jacks to permit free slip at this interface. Similarly the weight of each of the sample halves are supported below by three stationary jacks which have Teflon surfaced load bearing plates to permit easy horizontal motion of the blocks in response to the loading stresses provided by the flat jacks. Samples are Sierra White granite from Raymond, California. The fault surface was roughened using a specially designed frame and 30 grit as described in Okubo and Dieterich (1984). In the terminology of Okubo and Dieterich (1984), this is a 'rough' fault, having a peak to trough roughness of $\sim 80 \mu\text{m}$. This fault was so surfaced in the early 1980's. Based on estimated slip weakening distances, as detailed below, the change in roughness due to slip of this fault in experiments over the intervening twenty-three years is small.

There are two recording systems, one 12 bit system that runs continuously at 100 Hz and a triggered 12 bit system that records at 1 MHz for ~ 0.5 s about the trigger. Local shear stress is recorded close to the fault on 15 strain gage pairs equally spaced long strike (Table 1). The whole fault shear and normal stress are derived from transducers recording the pressure in the 2 independent sets of flat jacks. These two pressures are the principal stresses σ_1 and σ_3 ; the 45° degree angle between the loading faces and the fault yields $\tau = (\sigma_1 - \sigma_3) / 2$ and $\sigma_n = (\sigma_1 + \sigma_3) / 2$. The flatjack pressures when so converted to shear and normal stress on the fault are resolved to ± 0.02 MPa. Fault slip is recorded at 2 capacitive slip sensors crossing the fault approximately one third of the distance from the block center to the fault end in each direction. Accuracy of the slip sensors is $\pm 1.5 \mu\text{m}$, the precision is $\sim 0.3\%$. Particle motions are recorded on five, 2-component (fault shear and normal) accelerometer stations at 1 MHz. Fault normal motion was recorded near the block center with a single laser Doppler vibrometer. The location and recording rates of all sensors are listed in Table 1.

2.1. Loading and initial conditions

At different normal stresses between 4.0 and 8.0 MPa the fault was loaded by raising the shear stress at 0.001 MPa/s while holding the normal stress constant until an unstable shear failure of the fault occurs (Fig. 3) and propagating slip proceeds until the event self arrests. Rapidly accelerating slip is detected by an accelerometer and is used as an electronic trigger signal. The trigger causes the high speed transient waveform recorders to save the preceding 0.35 s of data, as they continue to record new data for 0.174 s following the trigger. The trigger also closes hydraulic control valves, preventing the servo control system from overcompensating as it attempts to respond to the sudden change in stress in the test apparatus. The low speed recording terminates 10 s after the trigger. Ideally the servo

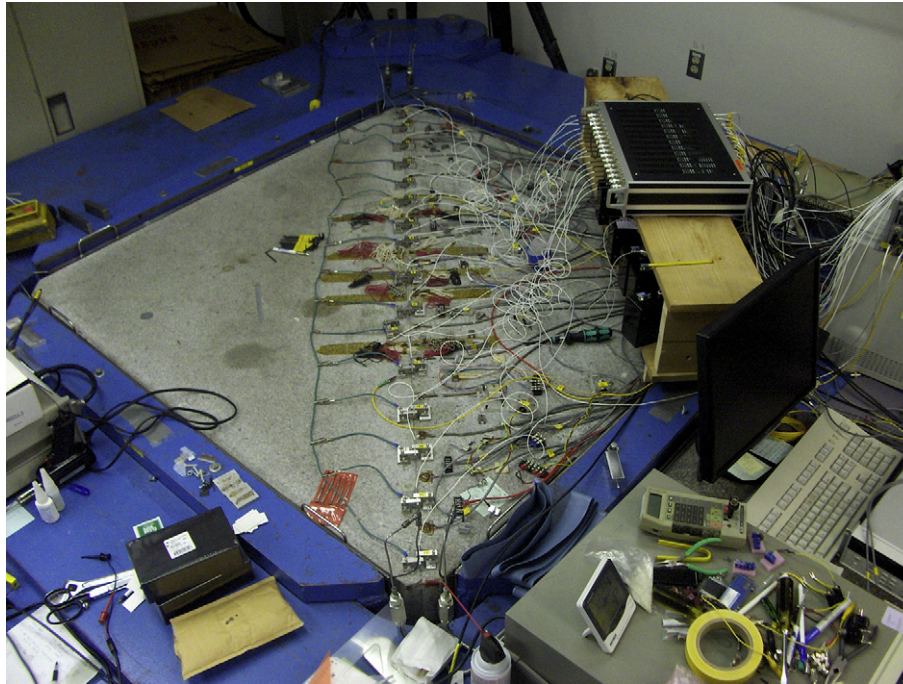


Fig. 2. USGS large biaxial faulting apparatus. Fault is 2 m long and 0.4 m deep. Instrumentation in the present experiments consists of 15 shear strain gages, 5, 2-component (shear and normal) accelerometers, 2 fault slip sensors and a single fault normal velocity sensor.

Table 1
Instrumentation.

x (m) along fault	y (m) off fault	Instrument	Description	100 Hz	10 ⁶ Hz
0.000	0.0		Fault end		
0.130	0.0119	sg_15	Strain gage	✓	✓
0.265	0.0119	sg_14	Strain gage	✓	✓
0.390	0.0127	sg_13	Strain gage	✓	✓
0.427	0.15	a9/a10	2 component accelerometer		✓
0.515	0.0141	sg_12	Strain gage	✓	✓
0.608	0.0	lp_2	Capacitive displacement	✓	✓
0.644	0.0136	sg_11	Strain gage	✓	✓
0.727	0.15	a7/a8	2 component accelerometer		✓
0.772	0.0136	sg_10	Strain gage	✓	✓
0.916	0.0143	sg_9	Strain gage	✓	✓
1.027	0.0	Fault center	Fault center		
1.027	0.15	a5/a6	2 component accelerometer		✓
1.027	0.15	v1	Laser vibrometer		✓
1.061	0.0144	sg_8	Strain gage	✓	✓
1.170	0.0136	sg_7	Strain gage	✓	✓
1.280	0.0128	sg_6	Strain gage	✓	✓
1.317	0.15	a3/a4	2 component accelerometer		✓
1.371	0.0	lp_1	Capacitive displacement	✓	✓
1.408	0.0135	sg_5	Strain gage	✓	✓
1.535	0.0114	sg_4	Strain gage	✓	✓
1.607	0.15	a1/a2	2 component accelerometer		✓
1.661	0.012	sg_3	Strain gage	✓	✓
1.787	0.0119	sg_2	Strain gage	✓	✓
1.925	0.0119	sg_1	Strain gage	✓	✓
2.055	0.0		Fault end		
0.5	0.5	σ_2	Pressure transducer	✓	
1.5	0.5	σ_1	Pressure transducer	✓	

control system would maintain static pressure in the loading jacks during the event, unfortunately the triggered valve closure is relatively slow, occurring in approximately 0.4 s. Furthermore, the response time of the servo system is slow relative to the duration of the dynamic rupture. Rupture takes roughly 2 ms for the shortest duration events whereas the servo system responds to stress changes in around 0.01 s, thus we have interpretable high speed records of dynamic strength loss, slip, and particle motion but some care must be taken to determine final values of stress, to account for post-event changes in loading induced by the servo controlled loading system prior to valve closure. Details of stress changes before, during and immediately following a dynamic event are described and illustrated in some additional detail in Appendix 1.

The fault surfaces are rougher than standard lab faults due to a difference between the 30 grit grinding compound used in preparation and the 60 grit for typical surfaces. A result is that the fault has a large slip weakening distance (Okubo and Dieterich, 1984), which in turn produces an approximately 1.5 m length nucleation patch, as discussed in more detail below. Although we are aware of no published observations of nucleation patch size for earthquakes or for laboratory faulting experiments, patch size can be inferred qualitatively from the experiments of Okubo and Dieterich (1984) and Ohnaka and Shen (1999). According to our experience, our observations are of a 'large' nucleation patch size; patch size is expected to be proportional to the fault's characteristic slip weakening distance (Dieterich, 1992; Ohnaka and Shen, 1999), equivalent to the average contact asperity size.

For this particular surface roughness, appreciable slip occurs prior to dynamic rupture in a region that is large relative to total fault dimensions. A significant portion of the fault is weakened prior to the onset of dynamic rupture; the extent of this region is apparent if all the shear strain gages are compared prior to failure (Fig. 3a and b). Low speed recordings suggest individual gages 4–9 have stress lower than the whole fault average (red) as measured at the loading jacks. Because the stress state at the time of rupture (initial stress) is inhomogeneous (Fig. 3a), the dynamic fault properties such as strength loss and fracture energy are

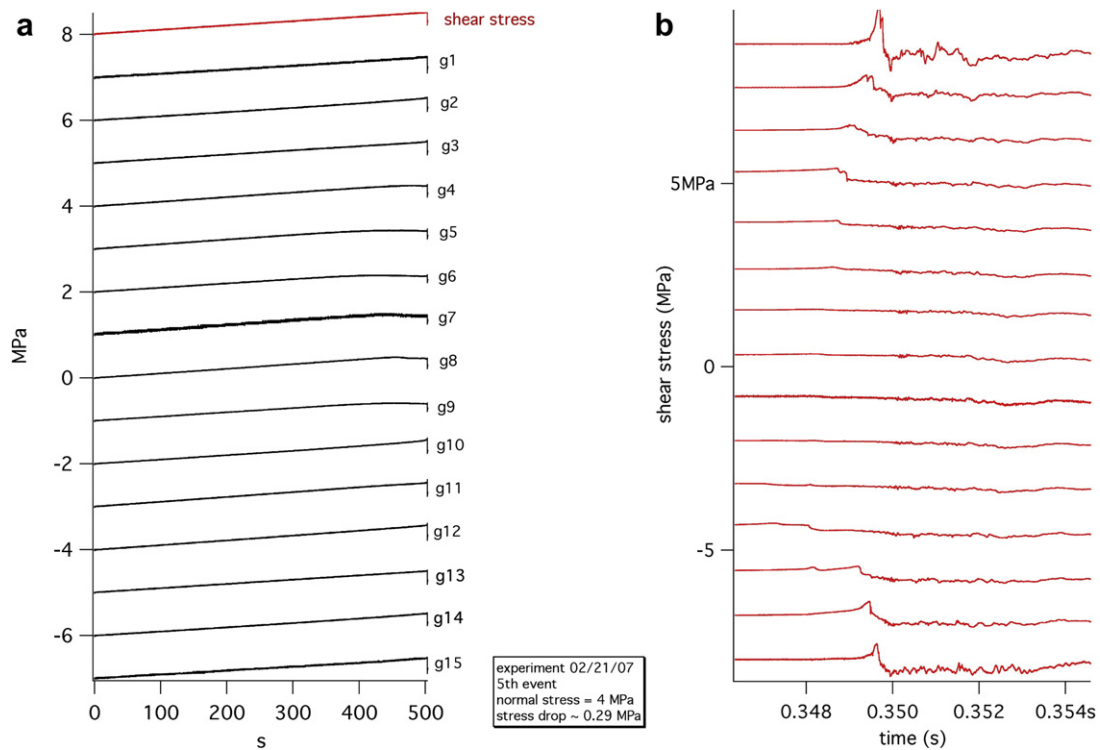


Fig. 3. Shear stress history of a single event. a) 100 Hz recording at the flat jacks (red) and 15 individual strain gauges (black). The strain gauges are offset by 1 MPa to give an approximate sense of spatial variation. Loading is at a constant stressing rate of 0.001 MPa/s, as measured at the loading jacks (red), until failure. Stress as recorded at the individual strain gauges shows a more complex behavior with the block centering undergoing precursory slip and having lower stress at failure while the ends remaining locked and have high stress at failure. Similarly, the stress drop is non-uniform. b) A portion of the 10^6 Hz recording of dynamic stress drop for the same event shown in a). Shear stress as recorded at the individual strain gauges during dynamic slip with the block center experiencing nearly no strength loss during the event and most of the strength loss being associated with the block ends. (For interpretation of the references to colour in this figure legend, the reader is referred to the web version of this article.)

inhomogeneous as well. For example Fig. 3a shows that stress drop at the fault ends is much larger than in the fault center. However, the extent of the nucleation patch appears even larger if the high speed records are examined (Fig. 3b). In these records there is appreciable dynamic stress drop only for the last 2 gages on each end of the fault, and even the gages 2 and 14 have smaller stress drops than at the gages nearest the fault end. This indicates that precursory slip extends to 0.20–0.25 m of the block end and a nucleation patch size of approximately 1.5 m. Thus, because of the large nucleation patch size relative to the total fault dimensions these ruptures have a non-homogeneous stress state before rupture and local source properties such as stress drop are not representative of the whole fault average.

3. Spatially averaged source properties measured and inferred from on-fault stress

We consider the average source properties, static stress drop, dynamic stress drop and strength loss from directly measured stress and inferred properties overshoot, seismic efficiency, and Savage and Wood's efficiency for comparison with analogous measurements from previous lab studies and natural earthquakes.

3.1. Stress

Shear stress measurements are made for all 73 events of this study at each of the 15 strain gauges. We record a static stress drop $\Delta\tau_s$ defined as the difference between initial τ_0 and final stress τ_1 . The initial stress is taken as the shear stress averaged over the first 0.00005 s of the high speed record (0.35 s prior to the trigger). The stress records contain long period oscillations of the press frame

that are initiated by the event and decay with time, so the final stress is overprinted somewhat by the starting and highest amplitudes of the frame oscillation. An additional complication is the response of the servo control system that increases the shear stress approximately linearly in time starting less than 0.01 s after the event. We correct for these effects by fitting the last 0.1 s of the high speed record to a linear relation and extrapolating back to the event end (see Figure A1 for an example). We record the fault strength loss $\Delta\tau$ defined as the difference between the yield strength τ_{yield} and the sliding strength $\tau_{sliding}$. For the sliding strength we use the shear strength time averaged over the last half of the event (Fig. 4). The dynamic stress drop is defined according to the standard seismological usage as the difference between the initial stress and the sliding strength. The stress overshoot is defined as the difference between the sliding strength and the final stress. Appendix 1 contains additional information on the procedures used to determine the stress parameters reported in this study. Table 2 lists these stress parameters; the average over all 15 gages for each event is used to construct the event average and then all the events at each normal stress are averaged. The strength loss, static stress drop, dynamic stress drop and stress overshoot each show weak pressure dependence (Fig. 5a).

The dependence of dynamic stress drop on normal stress (Fig. 5b) is similar to previous studies of dynamic rupture between bare surfaces of quartzofeldspathic rock at normal stresses in the range of 0.5–5 MPa (Okubo and Dieterich, 1981, 1984; Lockner et al., 1982; Lockner and Okubo, 1983) and at normal stresses up to 40 MPa (Johnson et al., 1973). Fig. 5b includes slope and intercept from linear regressions through these various datasets and the pressure dependence, the slopes of the data in Fig. 5b, ranges from 0.014 MPa/MPa upwards to 0.10 MPa/MPa (also see summary by

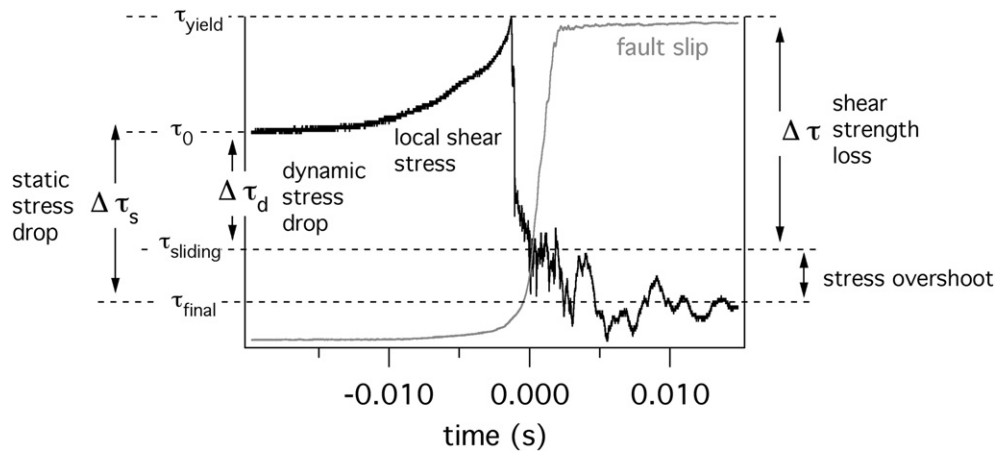


Fig. 4. High rate recording of local stress at a single strain gage (black) and slip (red) during an event. Key to the measured static stress drop $\Delta\tau_s$, dynamic stress drop $\Delta\tau_d$, strength loss $\Delta\tau$ and stress overshoot are shown. (For interpretation of the references to colour in this figure legend, the reader is referred to the web version of this article.)

Wong, 1986). Even without detailed contact scale observations it is reasonable to assume that the strength losses in our experiments are controlled by the same mechanisms as in these previous studies; principally shear induced dilatancy that reduces the real area of contact as slip accelerates (Scholz and Engelder, 1976).

Though Fig. 5b suggests general consistency between the existing studies there are differences with implications for extrapolating the results to the earth. The two weakest pressure dependencies (0.014, 0.027) are associated with our study and the rough fault results of Okubo and Dieterich (1984) that were conducted in the same apparatus and using the same fault we've used. If these data are extrapolated to the higher normal stresses in the Earth's crust the predicted stress drops are lower than those implied by the other studies cited in Fig. 5b by factors of 2–4, thus it is important to understand the cause of the low pressure dependence and further to determine whether these data are appropriate for comparison with large natural earthquakes.

The difference between the pressure dependence of stress drop observed by Okubo and Dieterich (1984) for smooth and rougher surfaces (0.061 and 0.014, respectively) is due to differences in precursory strength loss within the region of nucleation. The dimension of the nucleation patch is proportional to the characteristic slip weakening distance (e.g., Dieterich, 1992). Okubo and Dieterich (1984) found that the distance to weaken for their smooth and rough faults are 5 and 25 microns, respectively. Thus, we expect a nucleation patch five times larger for the rough fault. The nucleation patch is the region where the fault is partially to completely weakened prior to the onset of dynamic rupture (Fig. 3), implying dynamic stress drop up to 5 times smaller for the rough fault than for the smooth. The observed difference in dynamic stress drop of 4 times is consistent with this notion; the nucleation patch we observe is roughly 3/4 of the total fault dimension. For large earthquakes it is expected that the zone of nucleation is negligible relative to the final rupture dimensions (Johnston et al., 2006), therefore interpretation of our data

extrapolated to depth based on the pressure dependence must be made with some care.

An extrapolation of our stress drops to crustal stresses using 18 MPa normal stress/km for the depth range of 5–15 km predicts dynamic stress drops (Fig. 5b) between 2.5 and 7.3 MPa and static stress drops (Fig. 5a) of 2 and 5.9 MPa. These are in the range of typical for earthquakes of all sizes (Hanks, 1977; Allmann and Shearer, 2009).

3.2. Efficiency

As described in the Introduction, we compare energy partitioning in laboratory events to earthquakes without explicitly extrapolating in normal stress or scale by using the Savage-Wood efficiency. Although we might determine radiated energy from our accelerometer array there are some performance issues with these instruments. Fortunately, in contrast to typical earthquakes, we have constraints on energy release from near fault measurements of stress, fault strength change, stress drop and slip.

We do not have enough slip gages to determine the average sliding strength necessary to rigorously calculate overshoot in equation (5) so we use the time averaged shear strength $\tau_{sliding}$. Our estimate of stress overshoot

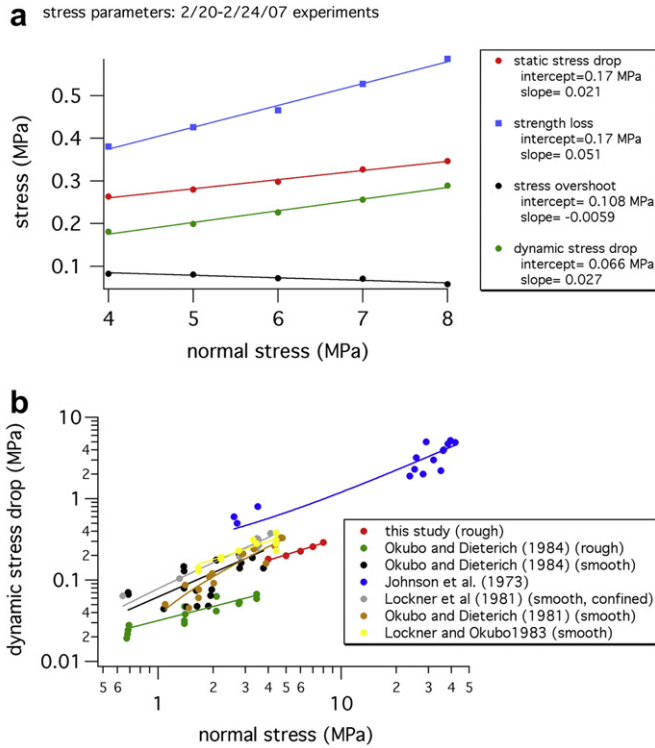
$$\xi \approx \frac{\tau_{sliding} - \tau_1}{\Delta\tau_s} \quad (6)$$

is adequate when the effective shear fracture energy is small relative to the energy per unit fault area available in the static stress drop ($\Delta\tau_s D$) and represents a lower bound on overshoot. The apparent stress τ_a is estimated using our approximate overshoot in (5). The seismic efficiency is $\eta = \tau_a / \bar{\tau}$; $\bar{\tau}$ is the displacement averaged shear stress. In these experiments the seismic efficiencies are low, mostly less than 2% (Table 2). Savage and Wood's efficiency is 0.27 (Table 2). Because of the sense of the error in our estimate of overshoot, these are upper bounds.

Table 2
Spatially averaged source properties derived from near fault stress.

σ_n (MPa)	N	$\Delta\tau_s$ (MPa)	$\Delta\tau$ (MPa)	$\Delta\tau_d$ (MPa)	Stress overshoot (MPa)	ξ	η_{sw}	η
4	8	0.263 ± 0.057	0.271 ± 0.059	0.181 ± 0.035	0.082 ± 0.023	0.309 ± 0.026	0.191	0.017
5	8	0.280 ± 0.040	0.288 ± 0.097	0.199 ± 0.028	0.081 ± 0.012	0.288 ± 0.006	0.212	0.016
6	23	0.298 ± 0.063	0.322 ± 0.101	0.224 ± 0.026	0.072 ± 0.025	0.237 ± 0.047	0.263	0.018
7	20	0.327 ± 0.093	0.344 ± 0.113	0.256 ± 0.068	0.071 ± 0.032	0.225 ± 0.048	0.275	0.019
8	14	0.346 ± 0.066	0.381 ± 0.106	0.289 ± 0.045	0.058 ± 0.058	0.156 ± 0.11	0.344	0.021

N is the number of measurements. The tabled values are the mean plus/minus the standard deviation of the N measurements. Individual uncertainties for the Savage-Wood efficiency can be estimated directly from those of overshoot ξ . Individual uncertainties are not listed for the seismic efficiency η ; those are between 0.002 and 0.005.



study	Intercept (MPa)	Slope (MPa/MPa)
this study	0.066	0.027
Lockner and Okubo 1983	0.057	0.061
Okubo and Dieterich (1984) smooth	0.001	0.061
Okubo and Dieterich (1984) rough	0.016	0.014
Okubo and Dieterich (1981)	-0.037	0.073
Lockner et al. (1981)	-0.007	0.085
Johnson et al. (1973)	0.15	0.10

Fig. 5. Pressure dependence of stress parameters. a) Pressure dependence of stress drop, strength loss, and stress overshoot. b) Comparison of pressure dependence of dynamic stress drop with results from previous studies.

We compare the Savage-Wood efficiency with earthquakes and previous experiments by comparing across many orders of magnitude in seismic moment ($M_0 = \mu DA$). Efficiency in these experiments is similar to prior lab events from Lockner and Okubo (1983) and with small mining-induced events compiled by McGarr (1999) (Fig. 6a). In comparing these lab and small earthquake efficiencies with large earthquakes we use data from Venkataraman and Kanamori (2004). Note that the Savage-Wood efficiency plotted in Fig. 6 is one-half the ‘radiation efficiency’ as defined by Venkataraman and Kanamori (2004). Large earthquake efficiencies (Fig. 6b) are more variable but if these data are representative of large earthquakes most events lie in the similar range of 0.1–0.5. Therefore, partitioning of radiated energy in our experiments is similar to earthquakes over a wide magnitude range and can be considered typical.

4. Additional representative source properties derived from fault slip time series

Using the slip time series we are able to measure additional source properties, event duration, average slip velocity, and infer the slip weakening distance and fracture efficiency. Whereas we have uniform and dense spatial coverage of stress change on the

fault from the near fault strain gages, our observations of fault slip are limited to two strategically-placed sensors. Each sensor is located approximately one third the distance from the fault center to the fault end. Placement was intended to capture a time history of slip that is representative of the spatial average of the fault and which can be differentiated to estimate the representative slip velocity time history. Acknowledging the limitations of these measurements of fault slip, nevertheless, in the following we treat these as representative.

4.1. Event duration and average slip velocity

In theory (1), the temporally averaged fault slip velocity is twice the near fault particle velocity (Brune, 1970), each being proportional to the fault strength loss or stress drop. To measure slip speed we use the high rate recordings from the 2 slip sensors. The analysis also produces an estimate of event duration. The slip speed and event durations reported below are the average of the two sensors.

Appreciable precursory slip is recorded on these instruments and often there is also measurable afterslip (Fig. 7) so it is difficult to define event onset and arrest unambiguously. As we are primarily interested in dynamic slip to the exclusion of precursory and afterslip, to determine the event duration and average slip rate we fit the slip vs time records with a piecewise linear function. The center segment is a Haskell-like source time relation with slope equal to the average velocity and starting and ending points defining the duration. When the resulting duration for all 73 events are plotted against the corresponding static stress drop (Fig. 8a) there is a strong systematic relationship. Low stress drop events have long duration and typical events are approximately 0.002s long; there are also suggestions of a minimum event duration and a minimum stress drop.

The time averaged slip event velocity versus static stress drop or versus strength loss for the 73 events are reasonably well represented by a linear relation, as would be expected from equation (1) or (2) (Fig. 8b). However, using the static stress drop, $\beta = 3000$ m/s, $\mu = 24000$ MPa and $V_r = 0.85\beta$, the slope is not consistent with either Brune’s or Ida’s theory (Fig. 8b); the average slip speed is certainly lower than predicted. Furthermore, unlike either theory the intercept is non-zero.

The relations among time-averaged velocity, event duration and static stress drop (Fig. 8a and b) can be understood using a simple analog, a slider block model (e.g., Johnson and Scholz, 1976; Rice and Tse, 1986), where, like Brune (1970), we ignore rupture propagation effects. For a slider block with abrupt strength loss and without radiation losses, there is a minimum slip duration related to the mass per unit area m and stiffness of the fault and loading system $\Delta t = \pi\sqrt{m/k}$. Since the time-averaged velocity can be expressed $\bar{V} = D/\Delta t$, and the total displacement as $D = \Delta\tau_s/k$, find that the maximum possible average sliding velocity is, $\bar{V} = \Delta\tau_s/k\Delta t$ (also see Johnson and Scholz, 1976; Okubo and Dieterich, 1984). Taking the known machine stiffness [3.3 MPa/mm, Lockner and Okubo, 1983] and the inferred minimum duration of 0.0018 s from Fig. 8a predicts the grey curve labeled ‘machine limit’ in Fig. 8b, not unlike the prediction of (1), having slope similar but slightly higher than the static stress drop observations but a zero intercept.

A slightly more sophisticated slider block model accounts for the gradual strength loss that defines the fracture energy. We use linear slip weakening

$$\tau = \tau_{yield} + \frac{\Delta\tau(d_* - \delta)}{d_*}, \quad \delta \leq d_* \quad (7)$$

$$\tau = \tau_{sliding}, \quad \delta > d_*$$

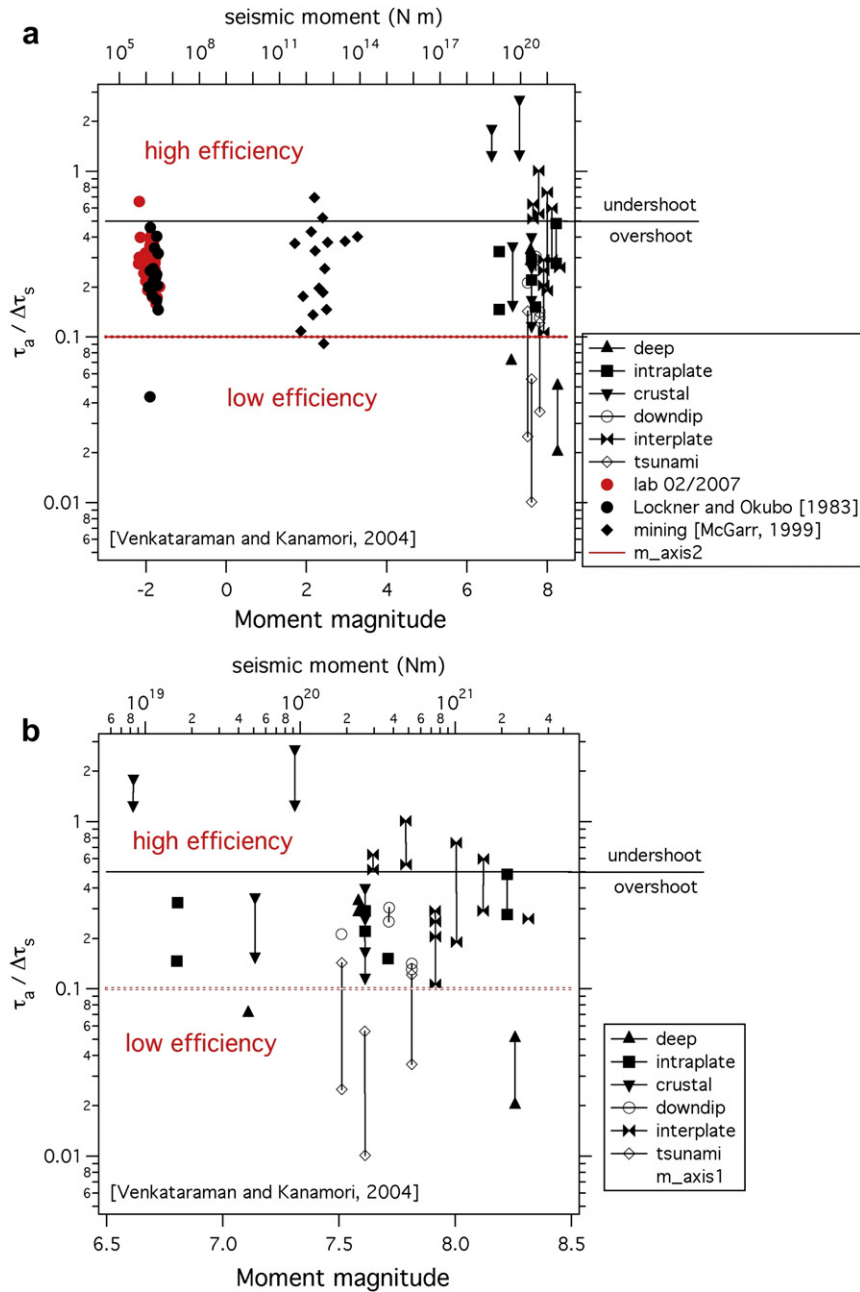


Fig. 6. Ratio of apparent stress to static stress drop for lab experiments and earthquakes. a) Lab events from this study and Lockner and Okubo (1983), mining events compiled by McGarr (1994, 1999) and large earthquakes from Venkataraman and Kanamori (2004). Horizontal lines define high, low and typical efficiency inferred from lab and mining-induced earthquakes (McGarr, 1994, 1999). Efficiency of 0.5 is the boundary between overshoot and undershoot. Note that the Savage-Wood efficiency plotted in this figure is one-half the 'radiation efficiency' defined by Venkataraman and Kanamori (2004). For the data of Venkataraman and Kanamori (2004), lines connecting points indicate the range in estimates of efficiency. b) Venkataraman and Kanamori's (2004) large earthquake data plotted on an expanded scale.

(Ida, 1972; Palmer and Rice, 1973) and include a radiation loss term $\mu/2\beta$ (Rice, 1993) in the equation of motion

$$k \left(\frac{\Delta t}{\pi} \right)^2 \frac{\partial^2 \delta}{\partial t^2} = \tau_{yield} - \tau - k\delta - \frac{\mu}{2\beta} \frac{\partial \delta}{\partial t}. \quad (8)$$

Equation (8) has an analytical solution described in Appendix 2. For simulations without fracture energy ($d^* = 0$) there is no minimum stress drop and all event durations are Δt . Simulations with fracture energy show the minimum duration and minimum stress drop (Fig. 9a) seen in the experiments. The displacement averaged velocity remains linear in static stress drop but now with non-zero intercept (Fig. 9b).

4.2. Estimated fracture energy and efficiency

Though the slider block model is a simplification of the experiments we believe the origin of the non-zero intercept in the model is the same as in the experiments. In this section we'll show that in-source dissipation from fracture energy produces a minimum possible stress drop and reduces the average dynamic slip velocity. Similar effects are expected for natural earthquakes.

For the linear slip weakening (7) fracture energy is

$$G_e = \frac{\Delta\tau d^*}{2}. \quad (9a)$$

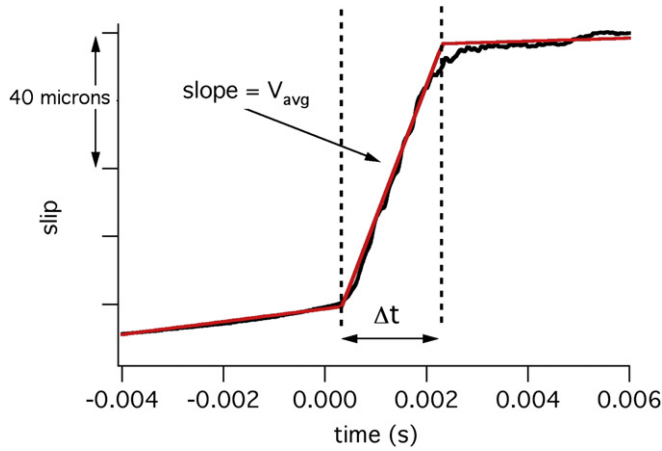


Fig. 7. Event duration and slip speed. Slip during the most rapid portion of an event. Shown also is a fit to the data used to determine the average sliding velocity and the event duration.

The fracture energy is proportional to the strength loss, as well as the slip weakening distance of the fault, thus, the fracture energy increases typically as the normal stress increases (e.g., Fig. 5a). Such a dependence of fracture energy on strength loss is generally expected for low temperature friction (e.g., Okubo and Dieterich, 1981; Andrews, 2005). The minimum strength loss for unstable

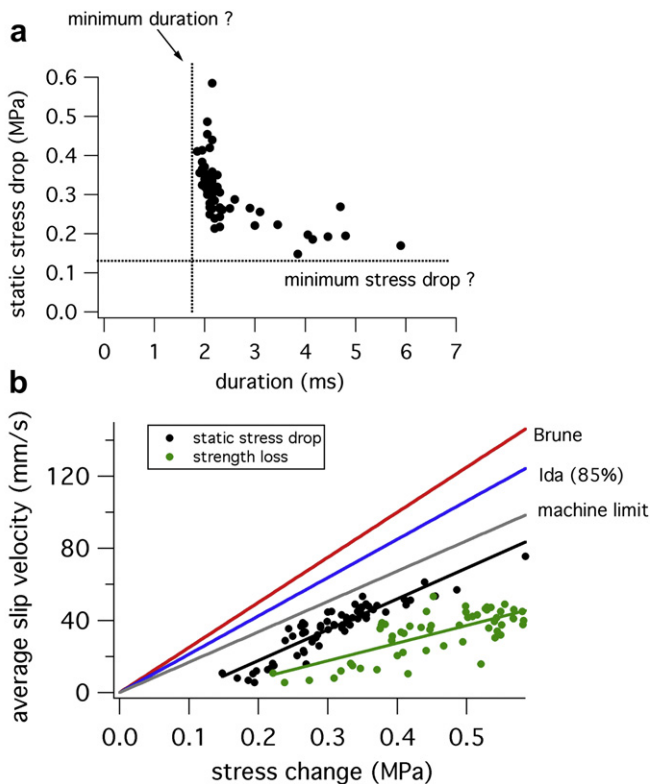


Fig. 8. Scaling of strength loss and static stress drop with event duration and slip speed. a) Event duration versus static stress drop. Dotted lines mark the apparent limits of the data. The data are qualitatively consistent with a minimum event duration and a minimum stress drop. b) Slip speed vs static stress drop (black) and strength loss (green). The black line is a fit to the static stress drop data with slope 177.1 mm/(s MPa) and minimum stress drop of 0.094 MPa. The green line is a fit to the strength loss data with slope 98.1 mm/(s MPa) and minimum stress drop of 0.121 MPa. Shown in red and blue are Brune's and Ida's theories (1) and (2), 250 and 212.5 mm/(s MPa), respectively. In grey is a line with slope 168.4 mm/(s MPa) $\{1/(\Delta tk)$ with $\Delta t = 0.0018$ s and $k = 3.3$ MPa/mm}.

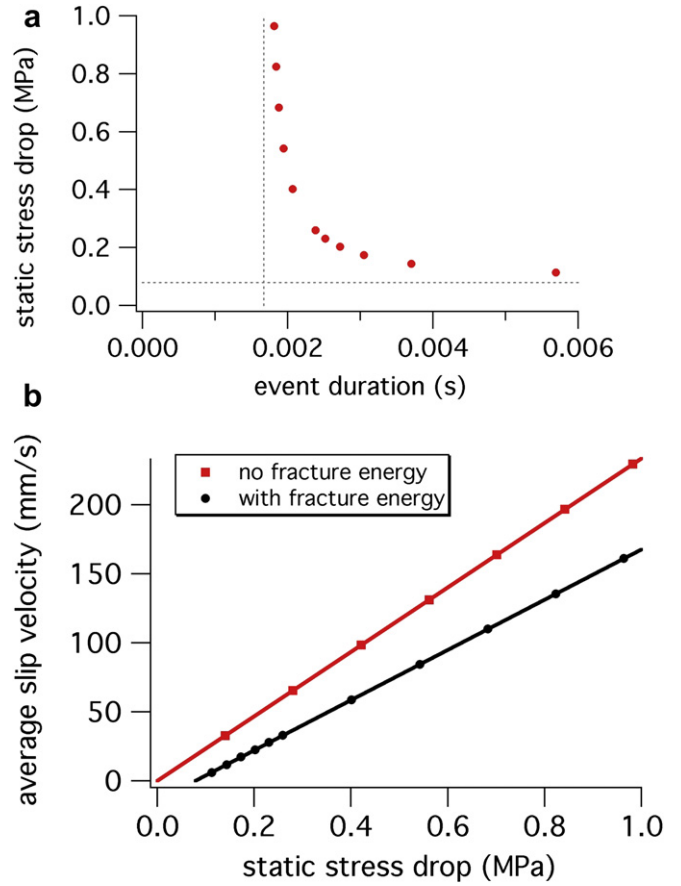


Fig. 9. Event duration and average velocity from simulation using a slider block model with radiation damping (8) (Rice, 1993) with linear slip weakening (7) for comparison with Fig. 8a and b. Parameters are $k = 3.3$ MPa/mm, $d^* = 25$ microns, $\beta = 3000$ m/s $\Delta t = 0.002$ s. If slider block simulations with radiation damping are conducted using the rock modulus and wave speed for the shear impedance in equation (8), slip is over-damped and the average slip speeds much smaller than observed. The shear impedance is apparently poorly defined for a slider block; in the calculation here $\mu = 7000$ MPa a) Duration. b) Velocity. Simulations are shown as symbols.

fault slip for a slider block is given by $\Delta\tau^{\min} = kd^*$. In the slider block model strength loss and dynamic stress drop are equivalent. At $\Delta\tau^{\min}$ dynamic stress drop and static stress drop are also equivalent. So in the context of the model, an average of the 2 regressions shown in Fig. 8b gives $\Delta\tau^{\min} = 0.11$ MPa and from the known machine stiffness (3.3 MPa/mm) we estimate $d^* = 33$ mm. This is similar to the average of 25 mm found by Okubo and Dieterich (1984) for the same rough fault we are using. The minimum fracture energy for these experiments predicted by the linear slip weakening model is

$$G_e^{\min} = \frac{kd_*^2}{2} = 1.8\text{J/m}^2. \tag{9b}$$

If we interpret the experiments using the linear slip weakening model with estimated d^* and our measured values of strength loss, fracture energy can be estimated for all events using (9a).

Though we argue here that fracture energy is an important quantity in influencing slip rate, and with analogy to dynamic rupture models (Andrews, 1976; Madariaga, 1976; Boatwright, 1980) where fracture energy controls propagation speed, because differences in scale and ambient stress between our experiments and the earth and for fracture energies inferred for large earthquakes (Rice, 1980; Wong, 1982; Rudnicki, 1980; Abercrombie and Rice, 2005) we use the fracture efficiency defined in the Introduction. The fracture

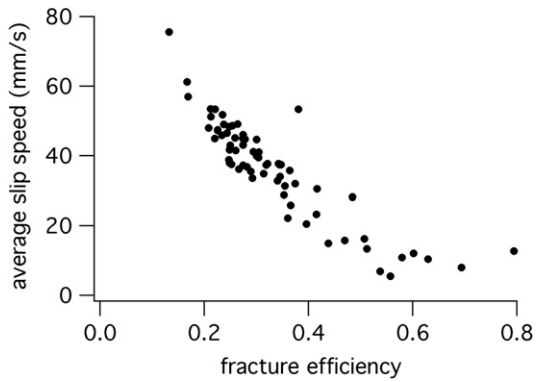


Fig. 10. Fracture efficiency calculated from measured strength loss and static stress drop using equations (9a) assuming $d^* = 33 \mu\text{m}$.

efficiency is calculated from our estimates of G_e (9a), and the measured values of slip and static stress drop. The average value of the fracture efficiency is 0.33; as this is of the same order and slightly larger than the Savage-Wood efficiency, the energy dissipated in fracture is large relative to the radiated energy in these experiments. Increases in fracture efficiency are clearly associated with decreasing average on-fault slip velocity (Fig. 10).

In so much as this efficiency can be estimated from seismological data, Abercrombie and Rice (2005) compiled earthquake source properties over a wide magnitude range and estimated fracture energy assuming no under or overshoot. A comparison with their published data (Fig. 11) does suggest that for some of our experiments fracture efficiencies are higher than for earthquakes in California, though the average is within the typical. Note also that our measurements of fracture efficiency are biased to high values. Fracture energy used in the estimate for fracture efficiency is calculated using equation (9a). So, it derives from strength loss measured coseismically, averaged from the 15 instruments in the strain gage array, and from d^* which we have estimated from the intercept in Fig. 8b. This value of d^* is likely near the maximum coseismic value of the slip weakening distance. Because the nucleation zone of the fault is large, significant precursory slip has already occurred over approximately $3/4$ of the fault. Coseismically within the nucleation zone the slip weakening distance should be shorter than d^* . Given this bias we believe that fracture efficiency in these experiments is consistent with that for typical earthquakes.

4.3. Peak slip velocity

Complete understanding of ground motion requires consideration of propagation effects and requisite local fluctuations in on-

fault slip rate that are not considered by using the event averages. Of particular interest are the most damaging motions from earthquakes which may be associated with the peaks in velocity and acceleration. Peak slip rate was determined from low-pass filtering the two slip sensors at the manufacturer's response limit (20 KHz) and differentiating (Fig. 12a). The reported peak velocity is the maximum velocity from the two different slip sensors. We've considered the relation between stress drop, strength loss and peak velocity. Peak slip velocity does not scale linearly with the average static stress drop, but does appear to be roughly linear with the average strength loss (Fig. 12b). The slope of the fit is much more similar to that predicted by (1) and (2) than the comparison with the average velocity (Fig. 8b). The intercept is again non-zero. Our interpretation of the peak velocities is complicated by end effects in the experiments. The ruptures in these experiments emanate from a large nucleation patch and intersect the block ends long before the cessation of slip. That is, in these experiments dynamic rupture initially, briefly involves true contained propagation but subsequently is dominated by back rupture from the free surfaces at the ends of fault. The arrival of back ruptures at the slip sensors coincides with the peaks in the velocity records. Because of these complications we are unable to directly relate the peak velocities measured in these experiments to natural earthquakes.

5. Discussion

The principal result from our measurements of strength loss and on-fault slip rate is that an equation of the form (0) is not appropriate for average near-fault particle velocity because of the contribution from fracture energy. There are two effects of the fracture energy seen in the experiments. First, is the non-zero intercept that arises from the minimum strength loss necessary for nucleation and propagation (Fig. 8b). The second effect is that the scaling of particle velocity with strength loss is weaker than expected from consideration of elasticity (equations (1) and (2)) due to energy loss to fracture energy on the fault. For our experiments, rather than (0), the relation between average particle velocity and strength loss is consistent with (3). Specifically, an empirical representation of the experiments in this study is

$$\dot{u} = (1 - m)(\Delta\tau - \Delta\tau^{\min}) \frac{\beta}{\mu}, \quad (10a)$$

where the intercept $\Delta\tau^{\min} = 0.11 \text{ MPa}$ and the empirical coefficient $0 \leq m < 1$. For our experiments $m = 0.3$, in other words the experiments predict a 30% reduction in average ground velocity due to the fracture energy within the source. For natural earthquakes the first effect in (10a) is not important but the second is as

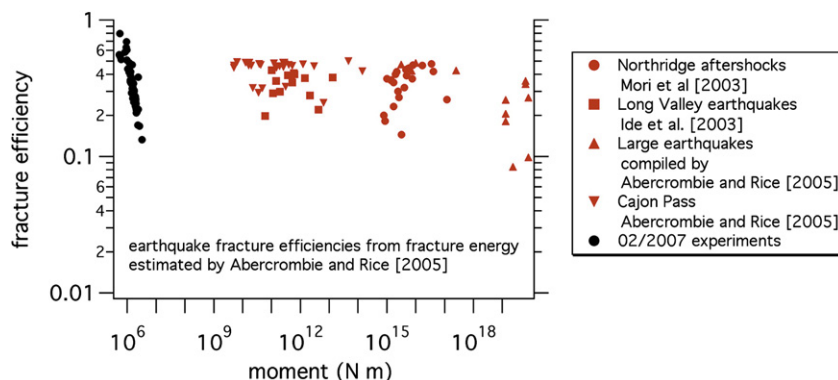


Fig. 11. Fracture efficiency for lab events and earthquakes in California. Earthquake data are from estimates of fracture energy and stress drop compiled by Abercrombie and Rice (2005).

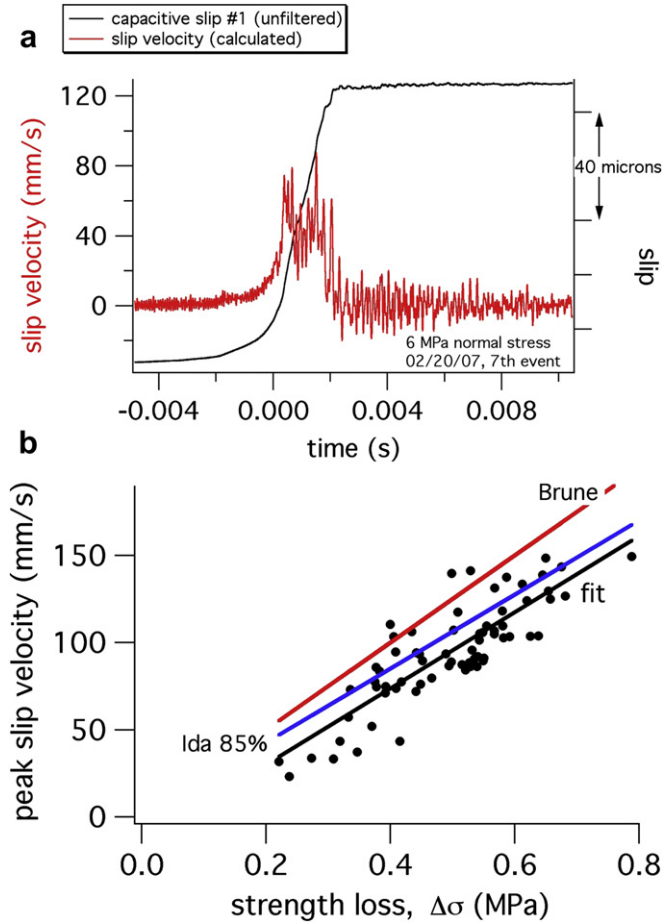


Fig. 12. Peak slip velocity as derived from slip sensor data. a) Example displacement and resulting velocity. To calculate slip rate the slip record was low pass filtered at 20 kHz prior to differentiation. b) Relationship between peak velocity and strength loss for the entire 73 event data set. Shown for reference is the prediction from (1) (red) and (2) (blue). The black line is a fit to the data.

in our experiments and as in theoretical calculations where on-fault and off-fault fracture energies are known to limit propagation rate and slip speed during dynamic rupture (Madariaga, 1976; Andrews, 1976). Using the notation of equation (0), for earthquakes we expect

$$\dot{u} = (1 - m)\Delta\tau \frac{V_c}{E}. \quad (10b)$$

From our comparison between the source properties of lab events and earthquakes we are able to explain typical earthquake source properties without resorting to thermal weakening within the source. The mechanism of strength loss underlying stress drop in our experiments is thought to be a small amount shear dilatancy which produces a dynamic reduction of contact area (e.g., Scholz and Engelder, 1976; Beeler, 2006). A secondary result of our study then is an implication that thermal weakening mechanisms are not the dominant processes determining fault strength during earthquakes. This idea has some support in naturally observed earthquake source properties, as follows.

As you would expect from recent high velocity faulting experiments [Di Toro et al., 2011], because large earthquakes have large slip and large slip rate there is a longstanding expectation that shear resistance during large earthquake slip is controlled by thermal processes such as melting and pore pressurization, not

present during small earthquakes (e.g., McKenzie and Brune, 1972; Lachenbruch, 1980; Mase and Smith, 1987). Ignoring conduction, latent heat, and radiated energy, assume that all the mechanical work of slip across a fault zone goes into increasing the temperature. The amount of heat ΔT produced during slip of $\Delta\delta$ is

$$\Delta T = \frac{\Delta\delta\bar{\tau}}{\rho\hat{c}w}, \quad (11a)$$

(Lachenbruch, 1980) where $\bar{\tau}$ is the average shear resistance, w is the width of the shearing portion of the fault and $\rho\hat{c}$ is the specific heat. For large earthquakes where slips are 1 m or more, shear heating would lead to dramatic changes in source properties (stress drop, efficiency, Savage-Wood efficiency, fracture efficiency) as slip increases if the shear thickness is less than a few centimeters (Lachenbruch, 1980). However, despite this expectation, the role of thermal weakening in large earthquake slip may be largely discounted because, instead of finding dramatic changes in earthquake source properties when the expected threshold for thermal weakening is reached, neither stress drop (Hanks, 1977) or apparent stress (Ide and Beroza, 2001) are found to be magnitude dependent. The absence of a thermal weakening signature in the stress drop data can be used as a constraint shear zone thickness within the earthquake source by replacing slip in equation (11a) with the static stress drop using the static stiffness of the rupture; for example for a circular rupture of diameter L , $\Delta\delta = 8\Delta\tau L/7\pi\mu$. Doing so produces:

$$\frac{w}{L} = \left(\frac{8\Delta\tau}{7\pi\mu\rho\hat{c}} \right) \frac{\bar{\tau}}{\Delta T} \quad (11b)$$

The parenthetical quantity in (11b) is a scale independent constant, consisting of material and geometric constants and stress drop. (11b) suggests that the thickness of coseismic shear zones increases with fault length unless the ratio of shear generated heat to shear strength $\bar{\tau}/\Delta T$ changes with scale. Restated, the structure of coseismic shear zones is self-similar if $\bar{\tau}/\Delta T$ is constant. The shear zone thickness to length ratio for our faulting experiments is artificial and is approximately the rms roughness of the fault surface divided by the fault length ($\sim 40 \mu\text{m}/2 \text{ m} = 2 \times 10^{-5}$). Despite being imposed, our width to length ratio implies a limit on natural shear heating of $\sim 250 \text{ }^\circ\text{C}$ at 12 km depth assuming drained conditions and hydrostatic pore pressure that is sufficient to explain the absence of thermal weakening observed in typical earthquake source properties.

Measurements of coseismic temperature change for natural faulting are non-existent as are measurements of coseismic shear resistance, and routine measurements of crustal stress and heat flow are rare. There are virtually no data on coseismic fault thickness or its scale dependence. In the absence of data and constraints, the predominant current thinking, argued by the theoretical fault modeling community, is that large earthquake rupture zones are extremely well localized, perhaps on the scale of less than 1 mm (e.g., Rice, 2006; Segall and Rice, 2006), an interpretation based on natural observations from select outcrops of a few shallow exhumed faults with large cumulative displacements (e.g., Chester and Chester, 1998). This is an interpretation that is not without qualification (Sibson, 2003). We make no contribution to the debate on coseismic shear zone thickness other than to point out the obvious, that scale independent stress drop precludes shear localization on the 1 mm scale for large earthquakes unless the shear resistance is inversely scale dependent. Restating the obvious, scale independent stress drop requires the average thickness of large earthquake coseismic shear zones is much larger than the interpretations based on Chester and Chester (1998) unless shear resistance is inversely scale dependent. Given a continued lack of investment in geophysical measurements of stress and heat flow,

geologic observations of shear zone structure will continue to be the primary source of knowledge upon which we base our understanding of large earthquake faulting.

6. Conclusions

The nucleation of slip in lab experiments during faulting on rough surfaces of bare rock at normal stresses between 4 and 8 MPa results in an inhomogeneous initial stress prior to dynamic rupture and a relatively high coseismic fracture energy. In our experiments at these conditions there is precursory slip within a nucleation patch that is nearly as large as the fault itself. The precursory slip reduces fault strength within the patch. As result the static and dynamic stress drops are small and increase weakly with normal stress (0.05 MPa/MPa). Average slip rate depends linearly on the fault strength loss and on static stress drop with a nonzero intercept. The average slip velocity is limited by an in-source energy dissipative contribution from on-fault fracture energy. The inferred linear slip weakening distance is 33 mm. Fracture energy is high relative to radiated energy. Seismic efficiency is low, less than 2%. The ratio of apparent stress to static stress drop is $\sim 27\%$, consistent with overshoot. The fracture efficiency is $\sim 33\%$.

Despite the complication of inhomogeneous initial stress and relatively high fracture energy these experiments have source properties (stress drop, slip velocity) that if extrapolated in normal stress are very similar to typical values for natural earthquakes of all sizes. Energy partitioning (radiated energy, overshoot and fracture energy) during these experiments is also very similar to earthquakes. Extrapolation of our laboratory results to simulate source parameters of earthquakes suggests that earthquake rupture processes are not affected by thermal weakening in any detectable way. This result is consistent with earthquake stress drops, for instance, that are scale independent which seems also to preclude a significant contribution from thermal weakening unless the ambient shear stress is inversely scale dependent.

Acknowledgments

Funding for some of the instrumentation used in this study was provided by USGS Venture Capital Fund. The laser vibrometer used was loaned to USGS by the Naval Postgraduate College. We are grateful for encouragement from Bill Ellsworth and scientific direction and consultation over a number of years from Jim Dieterich and David Lockner. Greg McLaskey, Brad Aagaard and Jack Boatwright provided detailed reviews which significantly improved the manuscript. This study was supported in part by the USGS Extreme ground motion research initiative funded by PG&E.

Appendix 1. Removing apparatus response from stress measurements

The fault is loaded by raising the shear stress at 0.001 MPa/s while holding the normal stress constant until an unstable shear failure of the fault occurs. Rapid acceleration recorded on an accelerometer triggers the high speed data recording system and initiates closure of the solenoid valves of the servo control system. The triggered valve closure occurs in approximately 0.4 s (Figure A2) and in the meantime the control system increases the shear stress approximately linearly in time starting less than 0.01 s after the event. An additional complication is the stress records contain long period oscillations of the press frame that are initiated by the event and decay with time (Figure A1). The procedure for determining the stress levels is first to determine the final stress. The event arrest is gradual. The end of the event is determined by fitting the slip vs time records at the two slip sensors with

a piecewise linear function (Fig. 7). The event end is chosen as the average from this analysis of the 2 slip gages. We correct for the servo response and the ringing of the apparatus by fitting the last 0.1 s of the high speed record to a linear relation and extrapolating back to the event end (Figure A1) to determine the final stress.

Appendix 2. Dynamic motion of a slider block with fracture energy and radiation loss

For a single degree of freedom spring-slider block, the equation of motion is the balance of the mass times acceleration against the difference between the spring force (here expressed as having units of stress $k(\delta_L - \delta)$) and the frictional resisting stress τ , less the radiated energy (here expressed as the radiation stress) $\chi d\delta/dt$:

$$\left(\frac{T}{2\pi}\right)^2 \frac{\partial^2 \delta}{\partial t^2} = (\delta_L - \delta) - \frac{\tau}{k} - \frac{\chi}{k} \frac{\partial \delta}{\partial t}. \quad (A1)$$

$T/2$ is the rupture duration in the absence of radiated energy, δ is slip on the fault, δ_L is load point displacement, k has units stress/displacement, $\chi = \mu/2\beta$, and μ is the shear modulus. The radiation damping term $\chi d\delta/dt$ is used to approximate energy lost as propagating seismic waves, here assumed to be planar waves (Rice, 1993). The particular choice χ is appropriate if β is the shear wave speed and all radiation results from shear waves. In (A1) the characteristic period is $T = 2\pi\sqrt{m/k}$. T is the half-period if the oscillator is undamped ($\chi = 0$) and if the effective fracture energy is negligible ($G_e \approx 0$).

To simulate the stress drop resulting from tectonic loading we assume that the spring load point is displaced at a constant rate V_L so that $\delta_L = \delta_{L0} + V_L t$, where δ_{L0} is the load point displacement at the onset of slip. The fault obeys linear slip weakening (7). When $\delta < d^*$, the solution of (A1) ($\chi = 0$) is given by

$$\delta = A \exp(r_1 t) + B \exp(r_2 t) + H V_L t - \frac{\eta V_L H^2}{k} \quad (A2a)$$

and

$$V = A r_1 \exp(r_1 t) + B r_2 \exp(r_2 t) + H V_L. \quad (A2b)$$

The substitutions used are $\delta_{L0} = \tau_f/k$ and $\Delta\tau_d/k = \delta_{L0} - \tau_k/k$, and

$$H = d^*k/(d^*k - \Delta\tau_d) \quad B = (-H V_L/r_1 - \eta V_L H^2/k)/(1 + r_2/r_1)$$

$$A = -B r_2/r_1 - H V_L/r_1$$

$$r_1, r_2 = -\frac{\eta}{k} \left(\frac{2\pi}{T}\right)^2 \pm \frac{\eta}{k} \left(\frac{2\pi}{T}\right)^2 \left[1 - 4 \left(\frac{kT}{\eta 2\pi}\right)^2 \left(1 - \frac{\Delta\tau_d}{d^*k}\right)\right]^{1/2}.$$

The solution

$$\delta = \exp(-Ft)(D \cos(f_w t) + E \sin(f_w t)) + V_L t - D \quad (A3a)$$

$$V = \exp(-Ft)[(-FD + E f_w) \cos(f_w t) - (FE + D f_w) \sin(f_w t)] + V_L, \quad (A3b)$$

is appropriate when $\delta > d^*$, and the constants F, D, E, f_w are determined from the solution of (A2a) and (A2b) when $\delta = d^*$. When the effective fracture energy is zero, the solution is given by (A3) and the constants are

$$D = \chi V_L/k - \Delta\tau_d/k \quad F = \chi/2k(2\pi/T)^2 \\ E = FD/f - V_L/f \quad f = \left(4[T/2\pi]^2 - [\chi/k]^2\right)^{1/2}/2[T/2\pi]^2,$$

(Beeler, 2001). The undamped solution to (A1), was first used in the context of laboratory stick-slip by Johnson and Scholz (1976), also see Scholz (1990).

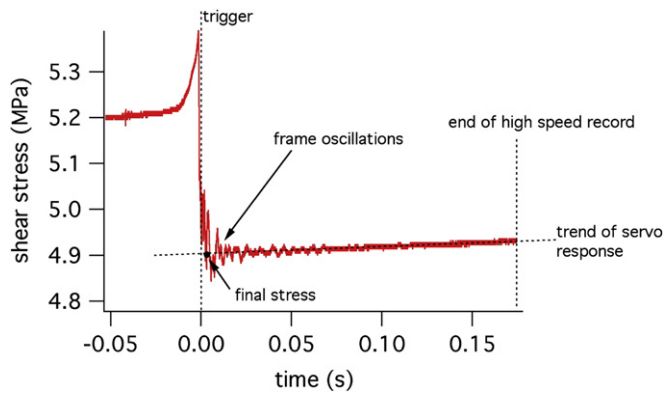


Figure A1. High speed record of shear stress on fault (g12). Shown in dashed lines are the trigger at 0.35 s, the end of the record at 5.24 s, and the stress trend from response of the servo system. Oscillations of the loading frame are induced by the stress drop and decay with time; these are labeled frame oscillations.

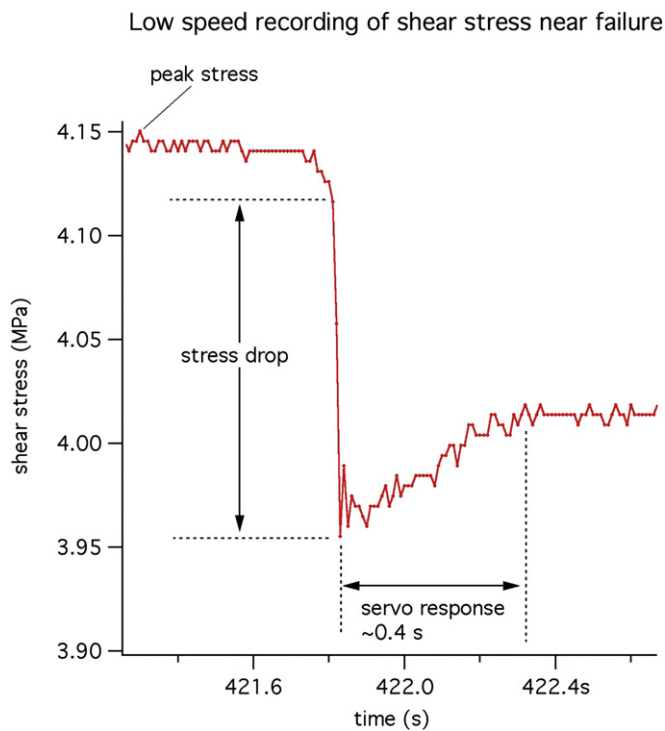


Figure A2. Low speed record of shear stress as measured from the flatjack pressures. This shows the servo response which lasts for approximately 0.4 s after the event.

References

- Abercrombie, R.E., Rice, J.R., 2005. Can observations of earthquake scaling constrain slip weakening. *Geophys. J. Int.* 162, 406–424.
- Allmann, B.B., Shearer, P.M., 2009. Global variations of stress drop for moderate to large earthquakes. *J. Geophys. Res.* 114. doi:10.1029/2009JB005821.
- Andrews, D.J., 1976. Rupture propagation with finite stress in anti-plane strain. *J. Geophys. Res.* 81, 3575–3582.
- Andrews, D.J., 2005. Rupture dynamics with energy loss outside the slip zone. *J. Geophys. Res.* 110. doi:10.1029/2004JB003191.
- Beeler, N.M., 2001. Stress drop with constant, scale independent seismic efficiency and overshoot. *Geophys. Res. Lett.* 28, 3353–3356.
- Beeler, N.M., 2006. Inferring earthquake source properties from laboratory observations and the scope of lab contributions to source physics, in *Earthquakes: radiated energy and earthquake physics*. In: Abercrombie, R., McGarr, A., Kanamori, H., Di Toro, G. (Eds.), *Geophysical Monograph*, 170.
- Boatwright, J., 1980. A spectral theory for circular seismic sources; simple estimates of source dimension, dynamic stress drop, and radiated seismic energy. *Bull. Seismol. Soc. Am.* 70, 1–27.

- Brune, J.N., 1970. Tectonic stress and the spectra of seismic shear waves from earthquakes. *J. Geophys. Res.* 75, 4997–5009.
- Chester, F.M., Chester, J.S., 1998. Ultracataclastic structure and friction processes of the Punchbowl fault, San Andreas system, California. *Tectonophysics* 295, 199–221.
- Dieterich, J.H., 1981. Potential for geophysical experiments in large scale tests. *Geophys. Res. Lett.* 8, 653–656.
- Dieterich, J.H., 1992. Earthquake nucleation on faults with rate- and state-dependent strength. In: Mikumo, T., et al. (Eds.), *Earthquake Source Physics and Earthquake Precursors*. Elsevier, New York, pp. 115–134.
- Di Toro, G., Han, R., Hirose, T., De Paola, N., Mizoguchi, K., Ferri, F., Cocco, M., Shimamoto, T., 2011. Fault lubrication during earthquakes. *Nature* 471, 494–499.
- Hanks, T.C., 1977. Earthquake stress-drops, ambient tectonic stresses, and the stresses that drive plates. *Pure Appl. Geophys.* 115, 441–458.
- Heaton, T.H., 1990. Evidence for and implications of self-healing pulses of slip in earthquake rupture. *Phys. Earth Planetary Interiors* 64, 1–20.
- Ida, Y., 1972. Cohesive force across the tip of a longitudinal shear crack and Griffith's specific surface energy. *J. Geophys. Res.* 77, 3796–3805.
- Ida, Y., 1973. The maximum acceleration of seismic ground motion. *Bull. Seismol. Soc. Am.* 63, 959–968.
- Ide, S., Beroza, G.C., 2001. Does apparent stress vary with earthquake size? *Geophys. Res. Lett.* 28, 3349–3352. doi:10.1029/2001GL013106.
- Johnson, T., Wu, F.T., Scholz, C.H., 1973. Source parameters for stick-slip and for earthquakes. *Science* 179, 278.
- Johnson, T., Scholz, C., 1976. Dynamic properties of stick-slip friction of rock. *J. Geophys. Res.* 81, 881–888.
- Johnston, M.J.S., Borchardt, R.D., Linde, A.T., Gladwin, M.T., 2006. Continuous borehole strain and pore pressure in the near field of the 28 September 2004 M 6.0 Parkfield, Earthquake: implications for nucleation, fault response, earthquake prediction, and tremor. *Bull. Seismol. Soc. Am.* 96, S56–S72.
- Lachenbruch, A.H., 1980. Frictional heating, fluid pressure, and the resistance to fault motion. *J. Geophys. Res.* 85, 6097–6112.
- Lockner, D.A., Okubo, P.G., Dieterich, J.H., 1982. Containment of stick-slip failures on a simulated fault by pore fluid injection. *Geophys. Res. Lett.* 9, 801–804.
- Lockner, D.A., Okubo, P.G., 1983. Measurements of frictional heating in granite. *J. Geophys. Res.* 88, 4313–4320.
- Madariaga, R., 1976. Dynamics of an expanding circular fault. *Bull. Seismol. Soc. Am.* 66, 639–666.
- Mase, C.W., Smith, L., 1987. Effects of frictional heating on thermal, hydrologic and mechanic response of a fault. *J. Geophys. Res.* 92, 6249–6272.
- McKenzie, D., Brune, J.N., 1972. Melting of fault planes during large earthquakes. *Geophys. J. Roy. Astr. Soc.* 29, 65–78.
- McGarr, A., 1994. Some comparisons between mining-induced and laboratory earthquakes. *Pure Appl. Geophys.* 142, 467–489.
- McGarr, A., 1999. On relating apparent stress to the stress causing earthquake fault slip. *J. Geophys. Res.* 104, 3003–3011.
- Okubo, P.G., Dieterich, J.H., 1981. Fracture energy of stick-slip events in a large scale biaxial experiment. *Geophys. Res. Lett.* 8, 887–890.
- Okubo, P.G., Dieterich, J.H., 1984. Effects of physical fault properties on frictional instabilities produced on simulated faults. *J. Geophys. Res.* 88, 887–890.
- Ohnaka, M., Shen, L.-f., 1999. Scaling of the shear rupture process from nucleation to dynamic propagation: Implications of geometric irregularity of the rupturing surface. *J. Geophys. Res.* 104, 817–844.
- Palmer, A.C., Rice, J.R., 1973. The growth of slip surfaces in the progressive failure of over-consolidated clay. *Proc. Roy. Soc. Lond. A332*, 527–548.
- Rice, J.R., 1980. The mechanics of earthquake rupture, in *physics of the Earth's interior*. In: Dziwonski, A.M., Boschi, E. (Eds.), *Proceedings of the International School of physics "Enrico Fermi", course 78*, 1979. Italian Physical Society, North Holland Publ. Co, pp. 555–649.
- Rice, J.R., 1993. Spatio-temporal complexity of slip on a fault. *J. Geophys. Res.* 98, 9885–9907.
- Rice, J.R., 2006. Heating and weakening of faults during earthquake slip. *J. Geophys. Res.* 111. doi:10.1029/2005JB004006.
- Rice, J.R., Tse, S.T., 1986. Dynamic motion of a single degree of freedom system following a rate and state dependent friction law. *J. Geophys. Res.* 91, 521–530.
- Rudnicki, J.W., 1980. Fracture mechanics applied to the Earth's crust. *Ann. Rev. Earth Planet. Sci.* 8, 489–525.
- Savage, J.C., Wood, M.D., 1971. The relation between apparent stress and stress drop. *Bull. Seismol. Soc. Am.* 61, 1381–1388.
- Segall, P., Rice, J.R., 2006. Does Shear Heating of Pore Fluid Contribute to Earthquake Nucleation? 111. doi:10.1029/2005JB004129.
- Scholz, C.H., Engelder, J.T., 1976. The role of asperity indentation and ploughing in rock friction, I, asperity creep and stick-slip. *Int. J. Rock Mech. Sci. Geomech. Abstr.* 13, 149–154.
- Scholz, C.H., 1990. *The Mechanics of Earthquakes and Faulting*. Cambridge Univ. Press, New York, 439 pp.
- Sibson, R.H., 2003. Thickness of the seismic slip zone. *Bull. Seismol. Soc. America* 93, 1169–1178.
- Venkataraman, A., Kanamori, H., 2004. Observational constraints on the fracture energy of subduction zone earthquakes. *J. Geophys. Res.* 109. doi:10.1029/2003JB002549.
- Wong, T.-f., 1982. Shear fracture energy of Westerly granite from post-failure behavior. *J. Geophys. Res.* 87, 990–1000.
- Wong, T.-f., 1986. On the normal stress dependence of the shear fracture energy. In: Das, S., et al. (Eds.), *Earthquake Source Mechanics*. Geophys. Monogr. Ser., vol. 37. AGU, Washington, D.C, pp. 1–11.